

Fletcher, T.M. and Duraisamy, K. and Brown, R.E. (2009) Sensitivity of tail rotor noise to helicopter configuration in forward flight. In: 65th American Helicopter Society Annual Forum, 27-29 May 2009, Texas, USA.

<http://strathprints.strath.ac.uk/27494/>

Strathprints is designed to allow users to access the research output of the University of Strathclyde. Copyright © and Moral Rights for the papers on this site are retained by the individual authors and/or other copyright owners. You may not engage in further distribution of the material for any profitmaking activities or any commercial gain. You may freely distribute both the url (<http://strathprints.strath.ac.uk>) and the content of this paper for research or study, educational, or not-for-profit purposes without prior permission or charge. You may freely distribute the url (<http://strathprints.strath.ac.uk>) of the Strathprints website.

Any correspondence concerning this service should be sent to The Strathprints Administrator: eprints@cis.strath.ac.uk

Sensitivity of Tail Rotor Noise to Helicopter Configuration in Forward Flight

Timothy M. Fletcher*

Karthik Duraisamy†

Richard E. Brown‡

*Rotor Aeromechanics Laboratory
Department of Aerospace Engineering
University of Glasgow
Glasgow, G12 8QQ, United Kingdom*

Understanding the mechanisms that lead to the production of noise by tail rotors across a broad range of flight conditions and helicopter configurations remains an active area of research. Furthermore, designers require numerical models that are able to efficiently and accurately predict the acoustic signature of the helicopter. Predictions made using the Vorticity Transport Model in conjunction with a linear acoustics code, in which the Ffowcs Williams-Hawkings equation is solved for the sound pressure level on a horizontal observer plane beneath a scaled model of the Bo-105 helicopter, have been shown to compare well with measurements made during the HeliNOVI experiments. As the vertical distance between the tail rotor and the main rotor is reduced, the acoustic signature of the tail rotor changes considerably. Both the blade-vortex interactions that occur between the tail rotor blades and their tip vortices, and the interactions between the tail rotor blades and the tip vortices trailed behind the main rotor blades, act as major sources of loading noise. The work presented in the paper suggests strongly, however, that the apparent acoustic advantages of a tail rotor with a particular sense of rotation cannot be considered independently of the vertical location of the tail rotor with respect to the main rotor.

Nomenclature

c	airfoil chord
C_n	normal force coefficient, $F_n/\frac{1}{2}\rho c u_b^2$
C_T	main rotor thrust coefficient, $T/\rho\pi\Omega^2 R^4$
C_{T_t}	tail rotor thrust coefficient, $T_t/\rho\pi\Omega_t^2 R_t^4$
F_n	sectional normal force
M	sectional Mach number
R, R_t	main and tail rotor radii, respectively
S	vorticity source
T, T_t	main and tail rotor thrust, respectively
u	flow velocity
u_b	flow velocity relative to the blade
μ	advance ratio
ρ	density
ψ	rotor azimuth angle
ω	vorticity
ω_b	bound vorticity
Ω	main rotor rotational speed
Ω_t	tail rotor rotational speed

Abbreviations

BVI	blade-vortex interaction
MR/TR	main rotor and tail rotor
SPL	sound pressure level [dB]
VTM	Vorticity Transport Model

Introduction

The acoustic signature produced by conventional helicopters with a single main rotor and tail rotor (MR/TR) is of considerable interest to both the manufacturers and operators. Helicopters with conventional configuration constitute a large majority of the total number that are operating today. The military stand to benefit from operating helicopters with a lower observability, whilst civilian operators will achieve improved environmental acceptance over densely populated urban areas if the noise produced by helicopters is reduced.

The turbomachinery within the engines and the rotor drive and gearbox assembly are responsible for significant proportions of both the discrete-frequency and broadband noise produced by helicopters. In conventional helicopters, however, a considerable proportion of the radiated sound is produced by the main

*Post-doctoral Research Assistant, t.fletcher@eng.gla.ac.uk

† Lecturer of CFD, dkarthik@aero.gla.ac.uk

‡ Mechan Chair of Engineering, rbrown@aero.gla.ac.uk

and tail rotors. The proportion of main and tail rotor noise is highly dependent on the flight condition and on the subtleties of the helicopter configuration, and, by extension, on the extent and severity of the interaction between the main and tail rotors. A comprehensive survey of the many forms of aerodynamic interaction to which helicopters are susceptible is provided by Sheridan and Smith (Ref. 1). A detailed analysis of some of the problems arising specifically from the aerodynamic interaction between the main and tail rotors is given by Fletcher (Ref. 2).

The interaction between the main and tail rotors of a conventional helicopter is influenced significantly by the vertical location of the tail rotor with respect to the main rotor. The extent to which the vertical position of the tail rotor may be varied is constrained, in part, by safety requirements that stipulate a minimum acceptable ground clearance. The sensitivity of the noise produced by a tail rotor to its vertical location with respect to the main rotor is of particular significance, however, to designers who wish to optimize the configuration of the helicopter in order to reduce or eliminate peaks in sound pressure beneath the aircraft.

Comprehensive studies of the sensitivity of the noise produced by a tail rotor to its vertical location are rare. Flight tests were performed on the Westland Lynx by Leverton *et al.* (Ref. 3) in order to isolate the source of the distinctive ‘burble’ sound produced by the aircraft. The tail rotor on the initial production variants of the Lynx was mounted such that its blades rotated toward the nose of the aircraft at the top of the disk (or top-forward). In forward flight the tip vortices from the main rotor would pass close-to or across the tail rotor disk. The geometry of the Lynx was such that intense pulses of sound occurred at a frequency that correlated exactly with the frequency at which the tail rotor blades crossed through the main rotor tip vortices. Similar tests were performed on a Lynx which had its tail rotor modified to rotate in the top-aft sense, and the problematic amplitude and directivity of the radiated sound was alleviated.

The experimental work performed by Yin *et al.* and his colleagues formed a part of the pan-European HeliNOVI program (Ref. 4), which aimed to increase the data available for the validation of numerical aeroacoustics methods and to explore noise-reduction technologies. In contrast to Leverton’s findings, it was found that, in climbing flight and in level forward flight, the mean noise level of the helicopter was lower when the tail rotor had a top-forward sense of rotation than a top-aft sense of rotation. The reason for the discrepancy between the conclusions of the two studies is thought to be that the tail rotor of the Lynx helicopter was mounted in a considerably lower position with respect to the main rotor than that of the Bo-105. The aerodynamic interaction that occurred between the main and tail rotors of the Lynx helicopter resulted in the production of noise by the tail rotor

when operating in the top-forward configuration. The sources of noise that developed on the top-forward tail rotor as a result of MR/TR interaction were largely alleviated when the sense of rotation of the tail rotor was reversed. The MR/TR interaction manifests when the tail rotor blades intersect the tip vortices trailed behind the blades of the main rotor.

This paper aims to demonstrate the subtle relationship between the noise produced by the tail rotor of a conventional helicopter and both its sense of rotation and its vertical position. Aerodynamic simulations of a generic helicopter with a conventional configuration will be performed using the Vorticity Transport Model. The aeroacoustics of the helicopter will then be analyzed using a computational acoustics code. In order to validate the VTM-acoustics method, numerical predictions are compared extensively against measurements made during the HeliNOVI experiments.

Helicopter Aerodynamic Model

The aerodynamics of a generic helicopter with a single main rotor and tail rotor has been simulated using the Vorticity Transport Model (VTM) developed by Brown (Ref. 5), and extended by Brown and Line (Ref. 6). The VTM is a comprehensive rotorcraft model in which the flow field around the rotorcraft is computed by solving the time-dependent Navier-Stokes equation, in finite-volume form, on a structured Cartesian mesh enclosing the helicopter system. After making the physically realistic assumption of incompressibility within the wake, the inviscid Navier-Stokes equations are cast into the vorticity-velocity form

$$\frac{\partial}{\partial t}\omega + u \cdot \nabla\omega - \omega \cdot \nabla u = S. \quad (1)$$

The first two terms within the vorticity transport equation describe the changes in the vorticity field ω , representing the wake, as a result of advection and stretching by the velocity field, u . The source term

$$S = -\frac{d}{dt}\omega_b + u_b \nabla \cdot \omega_b \quad (2)$$

accounts for the production of vorticity in the flow as a result of the spatial and temporal changes in the bound vorticity distribution, ω_b , on the various lifting surfaces of the rotorcraft. In the current version of the VTM, the aerodynamics of the rotor blades is modeled using a version of lifting-line theory. The velocity field is related to the vorticity field by using a Cartesian fast multipole method to invert the differential form of the Biot-Savart law

$$\nabla^2 u = -\nabla \times \omega. \quad (3)$$

Use of the fast multipole method, in conjunction with an adaptive grid in which cells are only present within the calculation when the vorticity within them is non-zero, dramatically increases the computational efficiency of the scheme when compared to an equivalent

Table 1: Rotor Data

	Main Rotor	Tail Rotor
Number of blades	4	2
Rotor radius	R = 2m	R _t =0.192R
Chord	0.061R	0.193R _t
Twist	-8° (linear)	0°
Airfoil	NACA 23012	NACA 0012
Root cut-out	0.22R	0.42R _t
Rotational speed	Ω = 17.4Hz	Ω _t = 5Ω
TR location w.r.t.	(high)	0.049R
MR (+ve up)	(low)	-0.034R

calculation performed on a fixed grid. The method is rendered effectively boundary-free as cells may be created, when necessary, on a Cartesian stencil which extends to infinity, by invoking the assumption that there is zero vorticity outside the wake. Numerical diffusion of the vorticity in the flow field surrounding the rotorcraft is kept at a very low level by using a technique based on Toro’s weighted average flux method (Ref. 7) to advance Eq. (1) through time. This approach allows highly efficient multi-rotor simulations, and permits many rotor revolutions to be captured without significant dissipation of the wake structure. This is in strong contrast to the performance of more conventional CFD techniques based on the pressure-velocity-density formulation of the Navier-Stokes equations.

In this study, the helicopter is represented as a pair of rotors, oriented in a conventional fashion with their centers located at representative points within the flow. This idealization of the problem ensures that solely the effects of the interactions between the rotors are captured, uncomplicated by the presence of further aerodynamic interactions between the rotors and the fuselage or empennage. The principal parameters for the main and tail rotors are given in Table 1. The main rotor rotates counter-clockwise when viewed from above (the convention for American helicopters), hence the tail rotor produces a force to starboard in trimmed flight. The tail rotor is of a two-bladed teetering design, whilst the main rotor is articulated. The structural flexibility of the blades is neglected. The rotor thrust coefficients and main rotor disk tilt angles were selected to represent those used during the HeliNOVI tests (Ref. 4), and these values are listed in Table 2.

All of the helicopter configurations described in this paper were simulated in forward flight at an advance ratio of 0.275. In order to compare numerical predictions with the HeliNOVI experimental data, the isolated tail rotor, and MR/TR systems with top-aft and top-forward senses of tail rotor rotation were simulated. Aeroacoustic simulations have been performed of tail rotors with a top-forward sense of rotation that were mounted in two different vertical locations with

respect to the main rotor, the first representing the scaled model of the Bo-105 used during the HeliNOVI tests, and the second designed to reflect the geometry of the Lynx helicopter, as detailed in Table 1.

Computational Acoustics

The acoustic field of the rotor system is determined using Farassat’s formulation of the Ffowcs Williams-Hawkings equation (Ref. 8). The instantaneous acoustic pressure, $p_L(t)$, at a given observer location due to a discrete point force, F , moving at Mach number M , is given by

$$p_L(t) = \frac{1}{4\pi a_0} \left[\frac{\partial}{\partial t} \left(\frac{F_\tau}{r(1-M_\tau)} \right) + \frac{a_0 F_\tau}{r^2(1-M_\tau)} \right]_\tau, \quad (4)$$

where a_0 is the speed of sound, and r is the distance between the observer and the source. The term in the square bracket is evaluated at the source time τ (the time at which the sound was emitted). Since the blade surface in the aerodynamic model is represented by a series of panels, the force contributed by each panel is treated as a point acoustic source located at the collocation point of the panel. The noise produced by these sources is then propagated according to Eq. (4). The aerodynamic effects of blade thickness are introduced through a look-up table of airfoil characteristics, but the lifting-line model within the VTM otherwise assumes an infinitesimally thin blade. The thickness noise is thus modeled independently using a source-sink pair attached to each blade panel. Noise due to quadrupole terms is neglected in the present work. This coupled VTM-acoustics method has been used previously to predict the acoustics of the HART II rotor (Ref. 9), where good agreement between the computed pressure time-histories and sound pressure levels was demonstrated against experimentally measured data in three representative flight conditions involving strong blade-vortex interactions (BVIs).

Comparisons with HeliNOVI Experimental Acoustic Data

It is widely accepted that the principal sources of noise from a helicopter in cruise are the various blade-vortex interactions that may occur between the main and tail rotor blades, and the concentrated vortices that are trailed from their tips. Figure 1 illustrates some of the principal features of the aerodynamic flow field in which the helicopter is immersed. The epicycloidal wake structure generated by both rotors, illustrated at the left of Fig. 1 by rendering the main and tail rotor wakes separately, is largely periodic and highly recurrent. The concentrated vortices formed behind the tips of the main rotor blades loop around each other and, in time, coalesce to form yet larger ‘super

Table 2: Trim Conditions

	Isolated Tail Rotor	MR/TR (Top-Aft)	MR/TR (Top-Forward)
Main rotor thrust coefficient (C_T)	-	0.00524	0.00524
Tail rotor thrust coefficient (C_{T_t})	0.00383	0.00391	0.00436
Longitudinal disk tilt	-	6.4° nose-down	6.4° nose-down
Lateral disk tilt	-	0°	0°

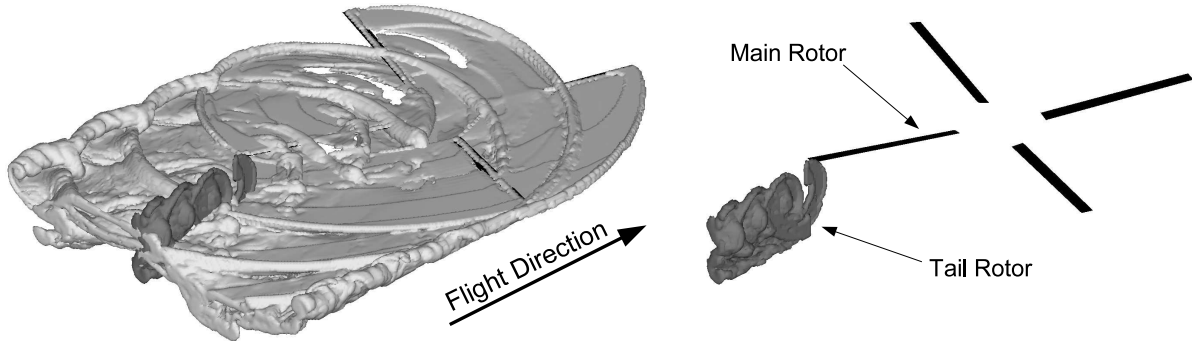


Figure 1: Wake of the MR/TR system, with a high tail rotor, in forward flight at an advance ratio of 0.275. Left: main (light contour) and tail rotor wakes. Right: location of the tail rotor wake relative to the main rotor.

vortices'. The tip vortices follow curved trajectories as they propagate downstream across the plane of the tail rotor, and are deformed considerably following their intersection by the blades of the tail rotor. When the helicopter operates at relatively high forward speeds, the evolution of the tail rotor wake is similar to that of the main rotor. The wake of the tail rotor differs, however, in the spacing between the tip vortices as they convect downstream and the spatial extent of the structure that they form. The structure of the wake developed by a high-mounted tail rotor, and its location with respect to the main rotor, can be inferred clearly from the diagram at the right of Fig. 1.

The remainder of this section will be dedicated to comparing of the sound pressure levels (SPL), predicted on a rectangular observer plane beneath the helicopter, with measurements made during the HeliNOVI tests. The locations of the observers correspond to the 16 x 16 array of inflow microphones used during the HeliNOVI tests, that are described by Yin *et al.* (Ref. 4). In Figs. 2–4, the overall SPL, composed of both the loading and the thickness noise components, is shown for each of the three combinations of helicopter configuration and flight condition given in Table 2. The amplitude of the main rotor noise that was computed using the VTM-acoustics method was found, for reasons that remain unclear, to be considerably larger than that measured during the HeliNOVI experiments, and is omitted from Figs. 2(b), 3(b) and 4(b). The consideration of only the noise produced by the tail rotor (in the frequency range of 5–40/main rotor revolution) is justified given

that it was found, in both the present work and by Yin during the HeliNOVI program, to be the dominant source of the noise generated by the helicopter.

A comparison of Figs. 2(a) and 2(b) shows that the computed directivity of the sound produced by the isolated tail rotor compares reasonably well with the experimental data. The location on the observer plane of the maximum in sound pressure is to the port side of the tail rotor, a short distance aft of the main rotor. A second peak in sound pressure is predicted to the starboard side of the tail rotor, approximately one tail rotor diameter aft of the equivalent peak in SPL measured during the HeliNOVI experiments.

A comparison of the measured and the predicted sound pressure distributions, given in Figs. 2(a) and 2(b), respectively, demonstrates that there is an under-prediction of the peak SPL by the VTM-acoustics method of approximately 5dB. It should be noted, however, that the aeroacoustic simulations performed during the current work omit several aspects of the test configuration that are known to affect both the amplitude and directivity of the noise produced by the helicopter system. In particular, neither the fin, or, perhaps more significantly, the fuselage and tail boom were modeled in the aeroacoustic simulations. Whilst the absence of the fuselage and empennage is likely to have had a relatively small effect on the principal sources of noise from the tail rotor in the high speed flight condition of interest here, the scattering and absorption of acoustic energy by these components of the helicopter would influence significantly the amplitude and directivity of the sound that is ra-

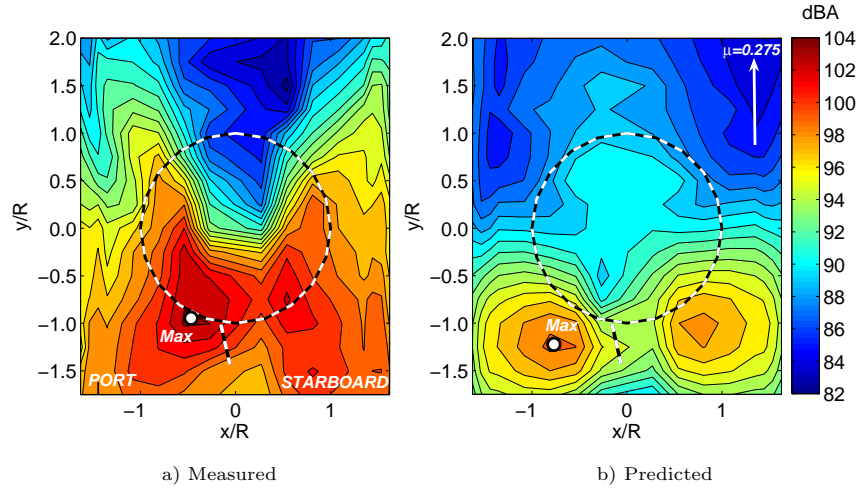


Figure 2: *A-weighted SPL (5–40/MR rev) in decibels for an isolated tail rotor with a top-aft sense of rotation in forward flight at an advance ratio of 0.275 (the positions of the rotors are shown for clarity).*

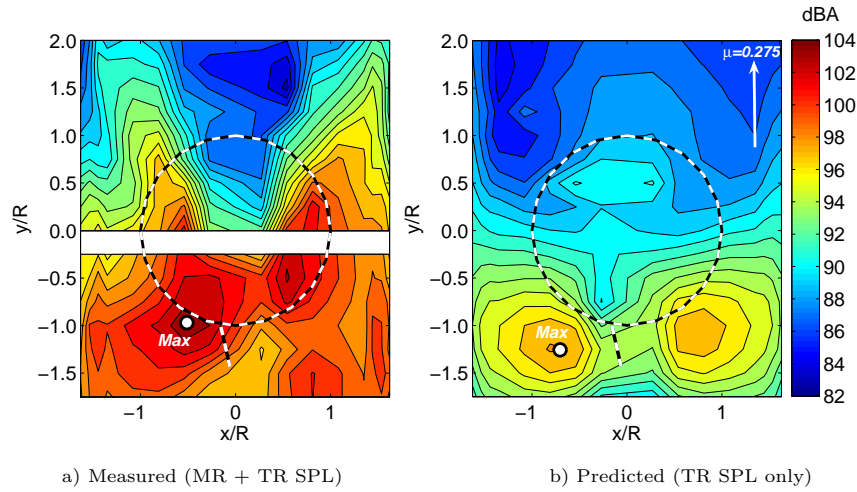


Figure 3: *A-weighted SPL (5–40/MR rev) in decibels for a MR/TR system with a tail rotor with a top-aft sense of rotation in forward flight at an advance ratio of 0.275 (the positions of the rotors are shown for clarity).*

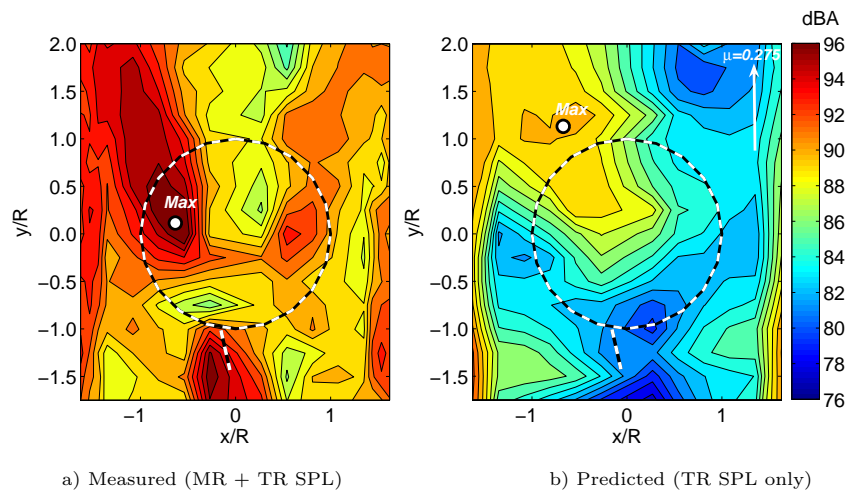


Figure 4: *A-weighted SPL (5–40/MR rev) in decibels for a MR/TR system with a tail rotor with a top-forward sense of rotation in forward flight at an advance ratio of 0.275 (the positions of the rotors are shown for clarity).*

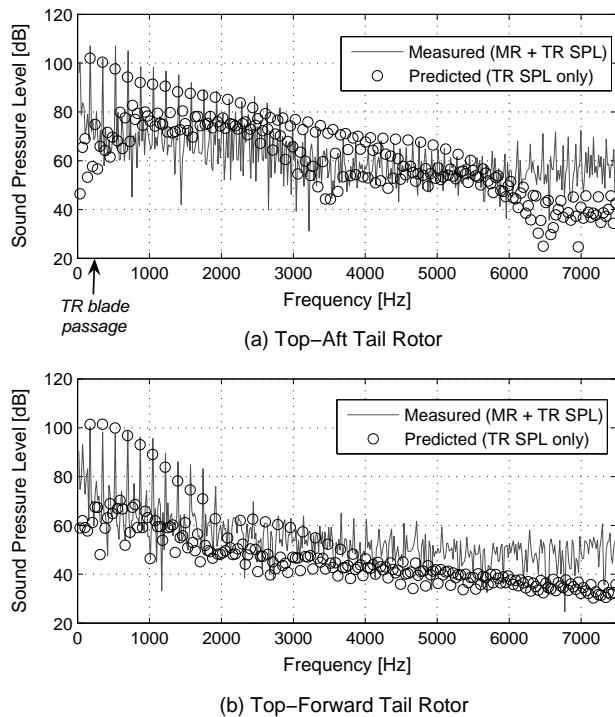


Figure 5: Noise spectrum at the locations of maximum noise, labeled ‘Max’, in Figs. 3 and 4, respectively, produced by MR/TR systems with opposing senses of tail rotor rotation.

diated toward the ground. Indeed, a comparison of the numerical and experimental data shown in Fig. 2 demonstrates how the SPL directly beneath the front half of the main rotor is over-predicted when compared to the experimental data, whilst the zones of high SPL that are measured on the observer plane, to either side of the shadow left by the fuselage, are not captured by the computational method. The combination of these two effects points markedly to the absence of scattering and absorption by the fuselage in the simulations.

A comparison of the measured and predicted sound pressure produced by the isolated tail rotor with a top-aft sense of rotation is shown in Fig. 2. A similar comparison is made in Fig. 3 for the top-aft tail rotor operating as part of a MR/TR system. The agreement between the predicted and measured distributions of SPL for the MR/TR system with a tail rotor rotating in the top-aft sense concurs with the comparison made in Fig. 2 for the isolated tail rotor configuration. This finding is, to a large extent, expected, given the marked absence of aerodynamic interaction between the main and tail rotors for this combination of helicopter configuration and flight condition.

Figure 4 shows a comparison of the measured and predicted noise produced by the tail rotor with a top-forward sense of rotation when operating as part of the MR/TR system. The significant difference in the directivity of the SPL that is evident for helicopter configurations with top-aft and top-forward tail rotors

is captured by the VTM-acoustics method. When operating as part of a MR/TR system, the top-forward tail rotor produces a zone of high SPL ahead of the main rotor, as shown in Fig. 4. In contrast, the top-aft tail rotor produces zones of high SPL to either side of the tail rotor, as shown in Fig. 3. The offset of approximately 5dB between the measured and predicted sound pressure levels at the locations of highest noise on the observer plane is consistent with the data presented in Figs. 2 and 3 for the helicopter configurations with a tail rotor that rotates in the top-aft sense. The distinct difference in the directivity of the sound pressure demonstrated by tail rotors with opposing senses of tail rotor rotation was shown by Fletcher *et al.* (Ref. 10) to result directly from the Doppler amplification of the loading noise produced by the rotors. The predicted acoustic signature does not include the region of high SPL almost directly beneath the tail rotor that is a characteristic of the measured noise data shown in Fig. 4(a).

The contours shown in Figs. 2–4 represent the sound pressure level computed by applying a band-pass filter (5–40/main rotor revolution) to the sound pressure signal in order to accentuate the noise that is caused by blade-vortex interactions. An indication of the ability of the VTM-acoustics method to capture the individual frequency components can be obtained by decomposing the SPL at particular locations on the observer plane into its constituent frequency components. Figure 5 shows the spectrum of sound pressure level at the locations of maximum SPL on the contour plots (labeled ‘Max’ in Figs. 3(b) and 4(b)) computed using the VTM-acoustics method for MR/TR systems with opposing senses of tail rotor rotation. Also shown in Figs. 5(a) and 5(b) are the spectra measured during the HeliNOVI experiments at the locations labeled ‘Max’ in Figs. 3(a) and 4(a). It should be noted that in Fig. 5, the spectra computed using the VTM-acoustics method represent the combination of loading and thickness noise produced only by the tail rotor. The frequency spectra measured during the HeliNOVI experiments are composed of the noise from all of the sources on the main and the tail rotors.

Figures 5(a) and 5(b) show that the sound pressure levels at those frequencies (less than 2kHz) that contribute the majority of the acoustic energy at the points of maximum SPL, shown in Figs. 3 and 4 respectively, are predicted well by the VTM-acoustics method. A slight under-prediction of SPL at these frequencies is observed but, in many cases, this under-prediction is less than 3dB. None of the principal frequencies are under-predicted by more than approximately 10dB. There is a notable under-prediction of the sound pressure level at frequencies above 6kHz for the top-aft tail rotor configuration, and above 4kHz for the top-forward tail rotor configuration, when compared with the experimental data. The sound pressure level generated at very high frequencies (4kHz or greater) is, predominantly, around 60dB or less, and

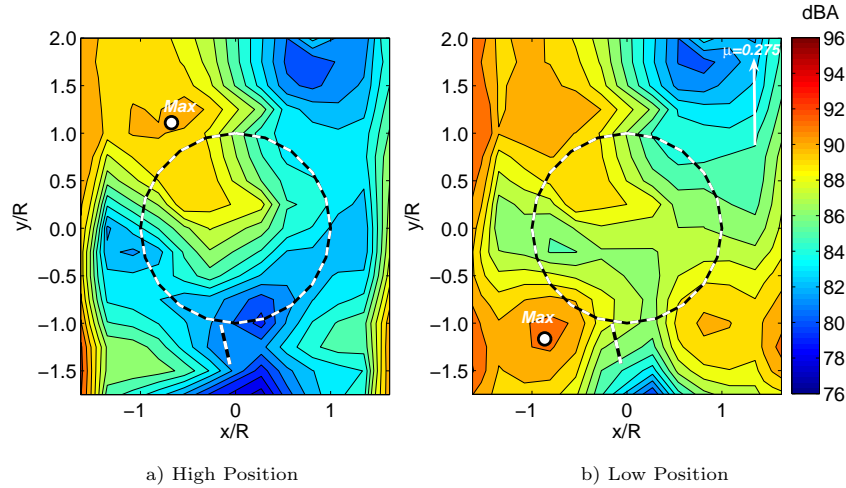


Figure 6: Predicted A-weighted tail rotor SPL (5–40/MR rev) in decibels for MR/TR systems with different tail rotor vertical locations in forward flight at an advance ratio of 0.275. Tail rotors in both cases rotate top-forward (the positions of the rotors are shown for clarity).

therefore contributes relatively little to the noise perceived by any particular observer located on the plane shown in Figs. 2–4. The inherent under-prediction of the high frequency sound by the VTM-acoustics method does not, therefore, significantly affect the overall sound pressure level that is computed at the observers located beneath the helicopter.

Sensitivity of Noise to Tail Rotor Vertical Location

In the HeliNOVI experiments, the sense of rotation, the tip speed, and the vertical location of hub with respect to the main rotor were varied in order to expose their effect on the noise produced by the helicopter, and hence, on the potential to achieve noise reductions. The rationale was effectively to reduce the noise created as a result of aerodynamic interaction between the main and tail rotors by removing the tail rotor from the main rotor wake in high speed forward flight. In this paper, however, the objective has been to lower the location of the tail rotor hub with respect to the main rotor so that it is similar to the geometry of the Lynx helicopter, and thus to induce interaction between the main and tail rotors.

Figures 6(a) and 6(b) demonstrate the effect on the directivity of the sound pressure produced by the tail rotor with a top-forward sense of rotation when it is lowered by a distance of 0.083R with respect to the main rotor compared to the configuration that was tested during the HeliNOVI program. Both figures show contours of sound pressure calculated at the same observer locations as those used to produce Figs. 2–4. The vertical locations of the observer points were lowered with respect to the main rotor by a distance equal to the change in tail rotor hub location

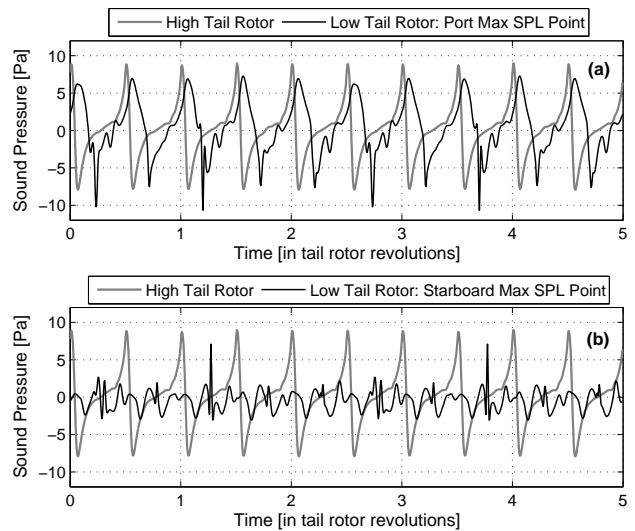


Figure 7: Sound pressure computed at the locations of maximum noise shown in Fig. 6 as a result of the loading on tail rotors in ‘high’ and ‘low’ positions in forward flight at an advance ratio of 0.275.

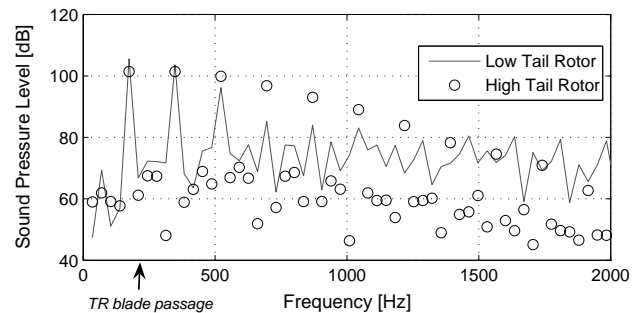


Figure 8: Predicted noise spectrum produced by tail rotors in ‘high’ and ‘low’ positions with respect to the main rotor at the locations of maximum noise, labeled ‘Max’, in Fig. 6.

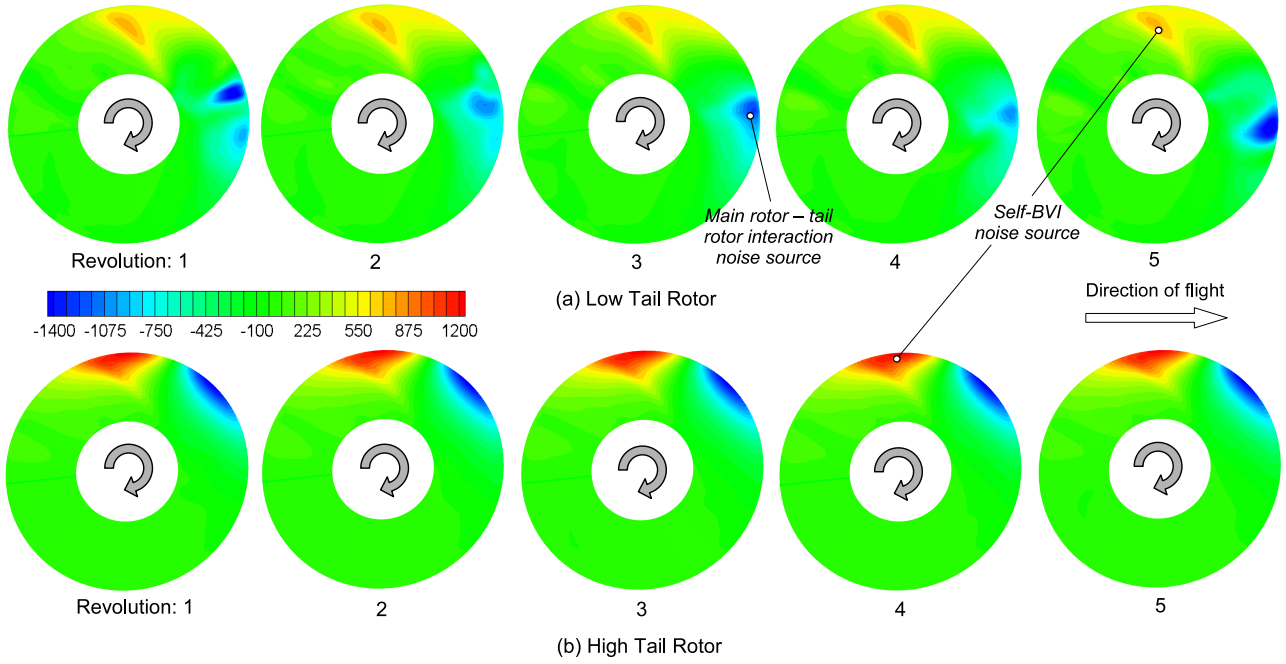


Figure 9: Acoustic source density (far-field component of loading noise, Pa/m^2) on a single blade of top-forward tail rotors in ‘high’ and ‘low’ positions with respect to the main rotor in forward flight at an advance ratio of 0.275, as evaluated at the maximum noise point labeled ‘Max’ in Fig. 6.

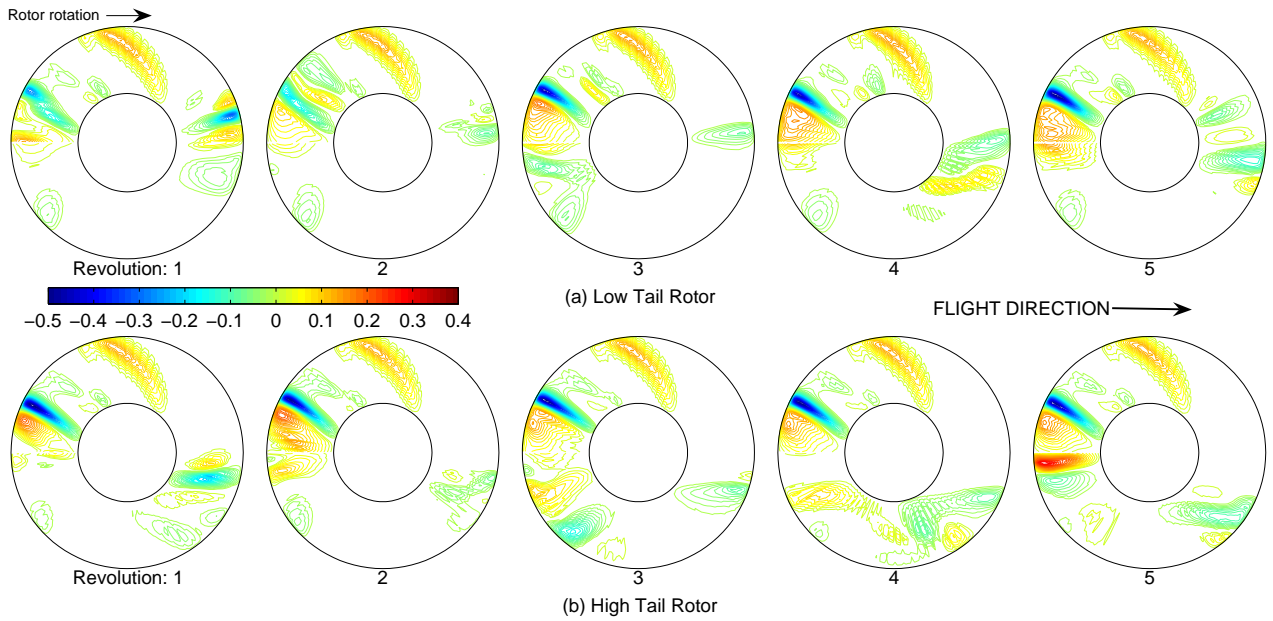


Figure 10: Acoustic sources on the tail rotor, represented by $d(C_n M^2)/d\psi$, in forward flight at an advance ratio $\mu = 0.275$.

when the SPL was computed for the low tail rotor. A comparison of Figs. 6(a) and 6(b) indicates the presence of two additional regions of high SPL on the observer plane beneath the rotor system, when the tail rotor is mounted in the low position, that are not produced by the tail rotor when it is mounted in the high position. The SPL at each of these points equals or exceeds that at the single peak in sound pressure level, located upstream of the tail rotor, shown in Fig. 6(a).

Figure 7(a) shows a comparison of the sound pressure at an observer located in the region of high SPL to the port side of the tail rotor (labeled ‘Max’ in Fig. 6(b)) with the sound pressure at an observer located in the region of high SPL ahead of the main rotor (labeled ‘Max’ in Fig. 6(a)). The dominant component of the pressure signal is that at the blade passage frequency of the tail rotor. The peak amplitudes of the sound pressure signals at each of the two ob-

server locations are very similar, as shown in Fig. 7(a). The sound pressure signal produced at the point of highest SPL on the port side of the ‘low’ tail rotor is more impulsive than the corresponding signal for the ‘high’ tail rotor. Figure 7(b) shows, again, the sound pressure produced by the high tail rotor, but it is compared with the sound pressure sampled at an observer located in the region of high SPL on the starboard side of the tail rotor, as shown in Fig. 6(b). On the starboard side of the tail rotor, the amplitude of the peaks in the pressure signal that occur at a frequency of two-per-tail rotor revolution is significantly smaller than that on the port side of the tail rotor. Figure 7(b) demonstrates the occurrence of impulsive peaks in the sound pressure at a frequency of two-per-main rotor revolution. An impulsive component of the sound pressure with a frequency of two-per-main rotor revolution is caused by an aerodynamic interaction between the main and tail rotors.

Figure 8 shows the spectra that are formed by decomposition of the sound pressure signal that is radiated to the locations of maximum noise, labeled ‘Max’ in Fig. 6, into discrete frequency components. Figure 8 demonstrates that the dominant frequencies (less than 1kHz) produced by the tail rotors in both the ‘low’ and the ‘high’ helicopter configurations are similar. The sound pressure levels associated with each of the principal modes generated by the high tail rotor are, however, significantly higher than the SPL of the principal modes generated by the low tail rotor. In contrast, the mean SPL across the range of frequencies shown in Fig. 8 is higher for the low-mounted tail rotor. This indicates that the sources of noise on the high and low tail rotors differ considerably.

Figure 9 shows the acoustic source density on the tail rotor that leads to the production of the sound pressure at the points of maximum noise labeled ‘Max’ in Fig. 6. The acoustic source density generated by one of the tail rotor blades is shown in Fig. 9 for five successive revolutions of the tail rotor. The principal sources of noise on the high tail rotor are periodic to the extent that they appear to be recurrent at the rotational frequency of the tail rotor, whilst those on the low tail rotor exhibit significantly greater unsteadiness.

The most significant source of noise on the low tail rotor is to be found at the leading edge of the tail rotor disk, as shown in Fig. 9(a). The precise distribution differs considerably between each of the five tail rotor revolutions shown in Fig. 9(a), however. Figure 10 shows the variation in loading with azimuth on one of the tail rotor blades as a function of the vertical position of the tail rotor with respect to the main rotor. The changes in loading are represented by the gradient $d(C_n M^2)/d\psi$, where C_n is the normal force coefficient at each blade section, and M is the local Mach number. Figure 10(a) shows that the acoustic sources that occur near the leading edge of the tail rotor disk in Fig. 9(a) are caused by abrupt changes in

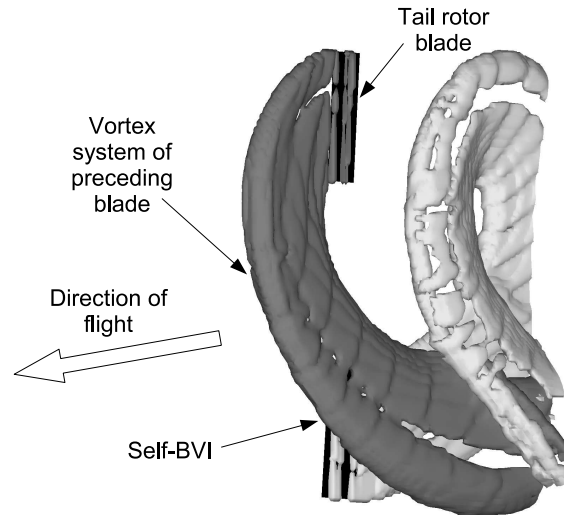


Figure 11: *Illustration of the interaction between a tail rotor blade and the vortex trailed from the tip of the preceding blade on the same rotor in forward flight at an advance ratio of 0.275.*

the loading on the blades. These impulsive changes in loading are caused by an interaction between the tail rotor blades and the concentrated vortices that are trailed from the tips of the main rotor blades. The data shown in Fig. 10(b) may be used to infer that an aerodynamic interaction occurs between the main rotor tip vortices and the lower half of the high tail rotor. The distinct change in the directivity of the sound pressure on the observer plane that is illustrated by a comparison of Figs. 6(a) and 6(b) suggests, however, that this interaction is a less significant source of noise on the high tail rotor than on the low tail rotor.

Both the low tail rotor and the high tail rotor generate an acoustic source at the top of the tail rotor disk (at an azimuth angle of approximately 90°), shown in yellow/red in Figs. 9(a) and 9(b). It is clear from Fig. 10 that this acoustic source is caused by a large gradient in the loading on the tail rotor blades that occurs at the same location on the rotor in every revolution. This azimuthal gradient in $C_n M^2$ is characteristic of a blade-vortex interaction that occurs between the blades of the tail rotor and the vortices trailed from their tips (self-BVI). The tail rotor self-BVIs occur at the blade passage frequency of the tail rotor (2/rev) and are created when a tail rotor blade passes near to the tip vortex trailed from the preceding blade on the rotor. A secondary noise source is present on the upper half of the high tail rotor. This source of noise is recurrent at the blade passage frequency of the tail rotor however, indicating that it is not caused by an interaction between the main and tail rotors.

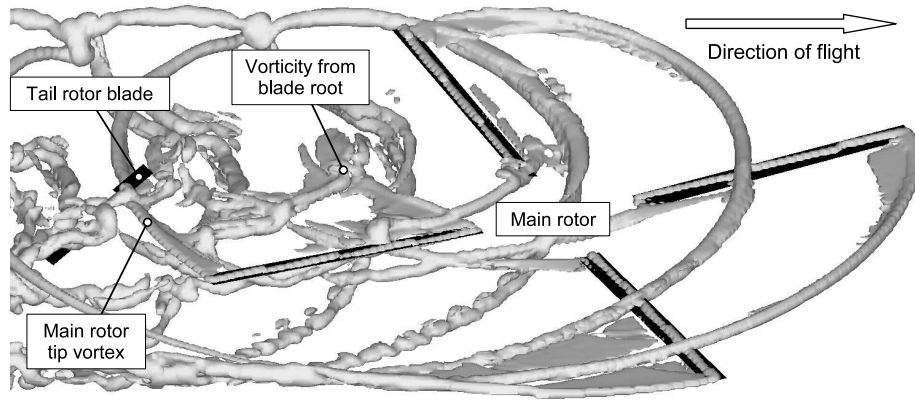


Figure 12: The wake developed by the main rotor in forward flight at an advance ratio of 0.275, as predicted by the VTM.

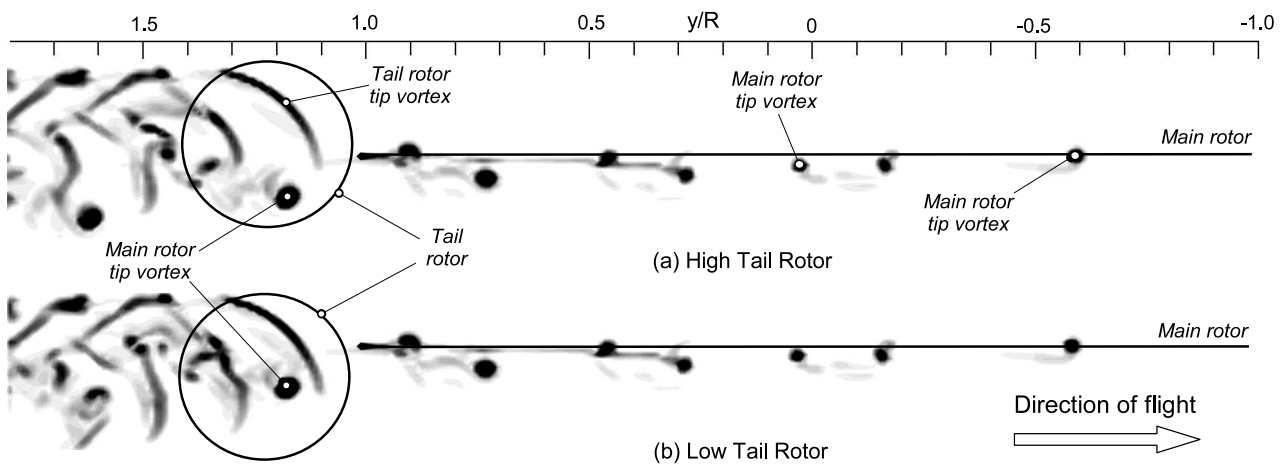


Figure 13: Comparison of predicted trajectories of the main and tail rotor tip vortices, represented using contours of vorticity magnitude on a plane through the wake located at a distance $0.11R$ to the port side of the aircraft centerline.

Tail Rotor Blade – Wake Interactions

The distribution of acoustic sources shown in Fig. 9 results, to large extent, from the impulsive loading associated with various blade-vortex interactions within the helicopter system. Figure 11 illustrates the blade-vortex interaction that occurs when the tip vortex trailed behind one of the tail rotor blades impinges on the following blade. This self-BVI manifests as a source of impulsive gradients in the loading on the tail rotor, as seen on the top half of the tail rotor disk in Fig. 10, and results in a significant proportion of the noise that is radiated by the tail rotor. The self-BVIs that occur on the tail rotor are largely independent of the main rotor and its wake, and therefore manifest on all of the helicopter configurations analyzed in this paper. Importantly, however, whilst the self-BVIs are the primary source of noise in each of the helicopter configurations in which the tail rotor is located in the

high position, they are only one of two distinct noise sources that exist when the same tail rotor is operated in the low-mounted position.

As the concentrated vortices trailed from the tips of both the main and tail rotor blades traverse in close proximity to the tail rotor, sharp gradients in loading are produced on the blades of the tail rotor. The mechanism by which interactions between the tail rotor blades and the surrounding vorticity field occur can be understood better by examining the structure of the wake that is developed by the MR/TR system. Figure 12 shows the wake developed by the main rotor of the helicopter, that has a tail rotor with a top-forward sense of rotation, in high speed forward flight. The concentrated vortices that trail from the tips of the main rotor blades can be seen clearly in Fig. 12 as filaments that follow a curved trajectory downstream of the main rotor. The vortices trailed from both the roots and the tips of the main rotor blades become tangled after convecting a relatively short distance downstream of the rotor. This phenomenon is particularly

pronounced on the retreating side of the main rotor, as shown in Fig. 12. The interaction between one of the two tail rotor blades and the concentrated vortex that is formed behind the tip of one of the main rotor blades can clearly be seen toward the left of the figure. As the tip vortices translate across the tail rotor, the natural instability of the vortex filaments is excited, and they no longer follow smooth curved trajectories as they propagate downstream from the tail rotor.

The locations of the tip vortices trailed by both the main and the tail rotors with respect to the tail rotor disk are clearly illustrated in Fig. 13. The figure shows the predicted trajectories of the main and tail rotor tip vortices, represented using contours of vorticity magnitude on a plane through the wake located at a distance $0.11R$ to the port side of the aircraft centerline. Figures 13(a) and 13(b) show the wakes developed by MR/TR systems with high and low tail rotors, respectively. The main rotor tip vortices pass approximately across the center of the tail rotor when it is mounted in the low position. In contrast, the main rotor tip vortices traverse across the tail rotor well below its the axis of rotation when it is mounted in the high position.

Figure 13 illustrates that the significant difference in the directivity of the sound pressure on the observer plane, for helicopters with tail rotors mounted in different vertical locations with respect to the main rotor (shown in Fig. 6), arises from the relatively subtle change in the character of the interaction between the main and tail rotors. The aerodynamic interaction between the main and tail rotors results in additional sources of noise on a tail rotor with a top-forward sense of rotation, as shown by a comparison of Figs. 9(a) and 9(b). The sensitivity of the noise produced by the tail rotor to its vertical location with respect to the main rotor supports the conclusions drawn by both Leverton (Ref. 3) and Yin (Ref. 4) regarding the optimal sense of tail rotor rotation for the respective types of helicopter that they tested. Moreover, the results presented in this paper show that when designing a conventional helicopter to produce the lowest noise signature, the sense of tail rotor rotation cannot be considered in isolation from the vertical location of the tail rotor with respect to the main rotor.

Conclusion

Aeroacoustic simulations of a conventional helicopter with a single main rotor and tail rotor have been performed using the Vorticity Transport Model, together with a linear acoustics code in which the Ffowcs Williams-Hawkings equation is solved for the sound pressure level on a horizontal observer plane beneath the helicopter. Predictions of the sound pressure level have been compared with measurements made during the HeliNOVI experiments. The VTM-acoustics method has been shown to provide good predictions

of the directivity and the amplitude of the SPL on the observer plane. Precise agreement between the sound pressure levels measured during the HeliNOVI experiments and the predictions made in this paper is restricted, in part, by difficulties in representing the scattering and absorption of acoustic energy by the fuselage, empennage and drive system that were present during the wind tunnel tests.

The interactions between each of the tail rotor blades and the tip vortices trailed from the preceding blades of the tail rotor (or self-BVIs) constitute a significant source of aerodynamically-induced loading noise produced by the helicopter. Aerodynamic interaction between the main and tail rotors is highly sensitive to the vertical location of the tail rotor with respect to the main rotor. The interactions between the tail rotor blades and the vortices trailed from the tips of the main rotor blades can result in a significant source of noise that is highly sensitive to the position of the tail rotor with respect to the main rotor. The work presented in this paper suggests strongly that the apparent acoustic advantages of a tail rotor with a particular sense of rotation cannot be considered independently of the vertical location of the tail rotor with respect to the main rotor.

Acknowledgments

The authors are very grateful to Dr Jianping Yin of the Deutsches Zentrum für Luft- und Raumfahrt (DLR) for his generosity in making available the experimental data presented in this paper.

References

- ¹Sheridan, P.F., and Smith, R.P., "Interactional Aerodynamics – A New Challenge to Helicopter Technology," *Journal of the American Helicopter Society*, Vol. 25, No. 1, 1980, pp. 3–21.
- ²Fletcher, T.M., and Brown, R.E., "Main Rotor – Tail Rotor Interaction and its Implications for Helicopter Directional Control," *Journal of the American Helicopter Society*, Vol. 53, No. 2, 2008, pp. 125–138.
- ³Leverton, J.W., Pollard, J.S, and Wills, C.R., "Main Rotor Wake/Tail Rotor Interaction," *Vertica*, Vol. 1, No. 3, 1977, pp. 213–221.
- ⁴Yin, J.P., Van der Wall, B., and Oerlemans, S., "Acoustic Wind Tunnel Tests on Helicopter Tail Rotor Noise (HeliNOVI)," *Journal of the American Helicopter Society*, Vol. 53, No. 3, 2008, pp. 226–239.
- ⁵Brown, R.E., "Rotor Wake Modeling for Flight Dynamic Simulation of Helicopters," *AIAA Journal*, Vol. 38, No. 1, 2000, pp. 57–63.

⁶Brown, R.E., and Line, A.J., “Efficient High-Resolution Wake Modeling using the Vorticity Transport Equation,” *AIAA Journal*, Vol. 43, No. 7, 2005, pp. 1434–1443.

⁷Toro, E.F., “A Weighted Average Flux Method for Hyperbolic Conservation Laws,” *Proceedings of the Royal Society of London, Series A: Mathematical and Physical Sciences*, Vol. 423, No. 1865, 1989, pp. 401–418.

⁸Farassat, F., and Succi, G.P., “The Prediction of Helicopter Rotor Discrete Frequency Noise,” *Vertica*, Vol. 7, No. 4, 1983, pp. 309–320.

⁹Kelly, M.E, Duraisamy, K., and Brown, R.E., “Predicting Blade Vortex Interaction, Airloads and Acoustics using the Vorticity Transport Model,” 9th American Helicopter Society Aeromechanics Specialists’ Meeting, Fisherman’s Wharf, San Francisco, USA, 23–25th January 2008.

¹⁰Fletcher, T.M., Duraisamy, K., and Brown, R.E., “Aeroacoustic Analysis of Main Rotor – Tail Rotor Interaction,” 34th European Rotorcraft Forum, Liverpool, UK, 16–18th September 2008.